

Design and analysis of an electrical magnetic holding device

Cheng-Yi Chen¹  · Rong-Ching Wu² · Bing-Jyun Tsai¹ · Chao-Ming Hsu³

Received: 26 April 2018 / Accepted: 15 June 2018 / Published online: 23 June 2018

© Springer-Verlag GmbH Germany, part of Springer Nature 2018

Abstract

Electromagnets are widely used as driving devices in industry. In this article, we describe various designs and methods of analysis for a built-in coil electromagnetic holding device based on three main design characteristics: volume, applied voltage, and suction force. Our aim is to achieve greater suction force or Gaussian value without changing the external dimensions of the frame, by varying the magnetic pole surface area, the thickness of the iron frame, and/or the electromagnetic material. We verify the design with the simulation software ANSYS Maxwell, which uses a commercial finite element method, to find the best design parameters to maximize the suction force or Gaussian value. The experimental results confirm the results of our simulation studies and demonstrate that simulations can achieve substantial reductions in cost and time over traditional trial-and-error methods. Furthermore, the experimental results indicate that electromagnetic products with bigger pole surface areas provide more suction force than electromagnetic products with smaller pole surface areas only when the applied voltage is less than 9 V. Above 9 V, smaller pole surface areas definitely result in bigger suction force.

1 Introduction

Electromagnets are devices that use electricity to generate magnetic fields and then use the generated magnetic fields to attract magnetic objects. Electromagnets differ from permanent magnets in that the former's magnetic fields are only generated when the electricity is on. In general, the strength of magnetic fields generated by electromagnets is related to the magnitude of the direct current, the number of

coils, and the properties of the magnetic material surrounded by the coils (Mansfield 2006). Electromagnets are widely used in industrial applications and in our daily lives; for example, electrical relays use small electrical currents to control the electromagnets of electrical switches, thus allowing one to control alternating currents with direct currents. Other examples include electromagnetic suction devices, which are based on the principle that magnetic fields are generated when direct currents are passed through electricity-conducting materials. The magnetic fields generated are then magnified by the magnetic materials located at the center of the devices and by the outer cavity to attract magnetic objects. Various designs and applications of electromagnets have been proposed and studied by Li et al. (2016), Wu et al. (2009), Zheng et al. (2015), and others.

The main application of electromagnets in industry is to attach objects. There are two major types of this application. The first is called electromagnetic suction devices and rely on electrical coils to generate magnetic fields. The second, called permanent suction devices, contains permanent magnets to provide permanent magnetic fields and electrical coils to generate magnetic fields that can either reinforce or cancel the permanent ones. Permanent suction devices are typically used to achieve long attachment times. This results in electrical savings of up to 95% compared with electromagnetic suction device under the same working conditions. On the other hand, for

✉ Rong-Ching Wu
rcwu@isu.edu.tw

Cheng-Yi Chen
k0464@gcloud.csu.edu.tw

Bing-Jyun Tsai
kes113325@gmail.com

Chao-Ming Hsu
jammy@kuas.edu.tw

¹ Department of Electrical Engineering, Cheng Shiu University, No. 840, Chengceng Rd., Niaosong Dist., Kaohsiung 83347, Taiwan

² Department of Electrical Engineering, I-Shou University, No. 1, Sec. 1, Syuecheng Rd., Dashu District, Kaohsiung 84001, Taiwan

³ Department of Mechanical Engineering, National Kaohsiung University of Science and Technology, No. 415, Chien Kung Rd., Sanmin Dist., Kaohsiung 80778, Taiwan

applications that involve frequent attachment and release, electromagnetic devices without permanent magnets are typically used. Regardless of the electromagnet used, the most critical components of the electromagnet are the coils that generate the magnetic field. In 2016, Alizadeh and Boulet (2016) presented their work on calculating the electromagnetic vector fields of symmetrical axis electromagnetic rings. Other published studies (Zheng et al. 2015; Sun et al. 2016; Liu et al. 2010; Zhu and Chang 2012) have also noted relevant computational methods, all of which are designed to rapidly calculate the vector fields of the electromagnetic coils to save development time and provide precise calculation results. The components of electromagnetic coils are simple, and research into each component has sought to accelerate product development.

Electromagnets are able to attract the objects due to the layout of their magnetic fields, so this plays an important role in the design of mechatronic devices. Han and Chang (2016) discussed how multiple coils in an electromagnet affect each other's magnetic fields. Other researchers (Liu et al. 2016; Kim and Chang 2007) have presented structural optimizations for other types of electromagnets. Han and Chang (2016) have looked at structural optimization for other types of electromagnets. The coils of electromagnets can be actuated using various driving methods, the most common of which is the linear driving method. For example, Mercorelli et al. (2003) proposed a linear drive to achieve a short stroke actuator. Note that the products developed with electromagnetic coils as their core technology often have stroke distance of 5–20 mm at most. Furthermore, Duchaud et al. (2015) conducted research on optimizing control modes for linear breaks in the two-stage valve of an automobile engine. Using Ansoft Maxwell finite element analysis of magnetic fields for system dynamic analysis, they reduced the valve size by 20% while maintaining the same power consumption. Wang et al. (2016) also discussed how changing the cross-sectional area of the iron core and coil current affected high-voltage electromagnetic valves' performance. Their system optimization design was based on ANSYS Maxwell finite elemental analysis of how changes in all parameters affected system performance.

The preceding examples indicate that applications of electromagnets encompass three major topics: the structure of electromagnets, external auxiliary devices, and control methods. In this article, we will focus on the analysis and design of electromagnetic holding devices, which are widely used in industry (see Fig. 1). Because the control technology and design of external auxiliary devices are quite mature already, we will focus on discussing the method of calculating how changes in parameters such as the magnet poles' cross-sectional area and the magnet frame wall thickness affect the maximum Gauss value of the electromagnet's surface and the electromagnet's

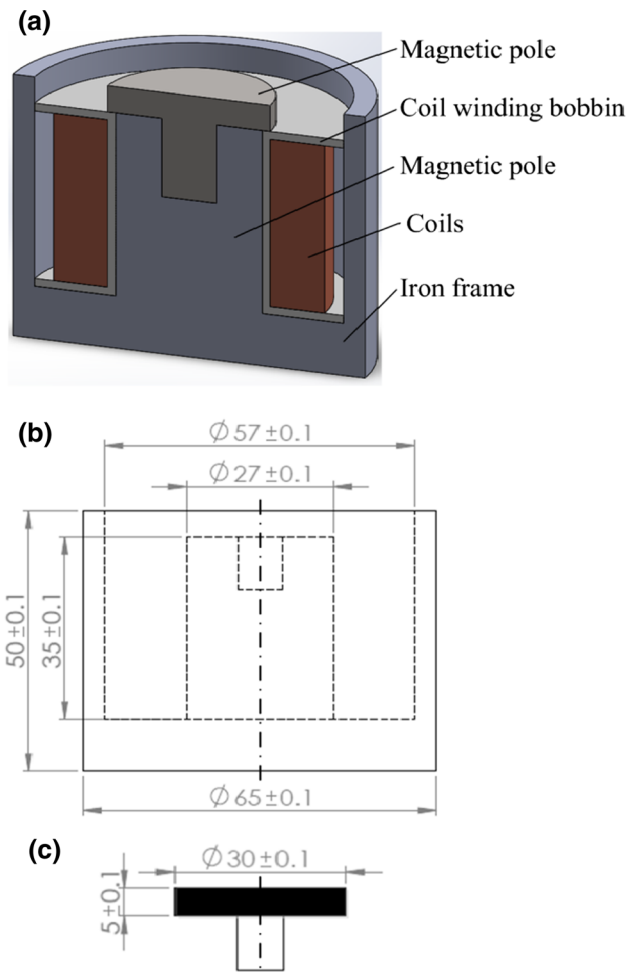


Fig. 1 Electromagnetic structure diagram: **a** 3D diagram, **b** dimensions for iron frame and coil parts, **c** separation design of magnetic pole

attachment weight. Based on the performance requirements of electromagnets, a customized design and analysis method will be presented to shorten the product design time and further decrease the product development cost.

2 Effect of magnet pole cross-sectional area on electromagnets

This article mainly discusses the traditional built-in coils of electromagnetic holding devices. This type of electromagnet is only magnetic when the electricity is on. A cross-sectional diagram is shown in Fig. 1, which includes the iron frame, axial line dimensions, and separation poles. The circular cross-sectional area of the magnetic pole is considered to be $\phi 55$ mm initially, as shown in the black area of Fig. 1a. We investigated the effect of the magnetic pole's cross-sectional area on the electromagnet's overall characteristics by gradually decreasing the cross-sectional

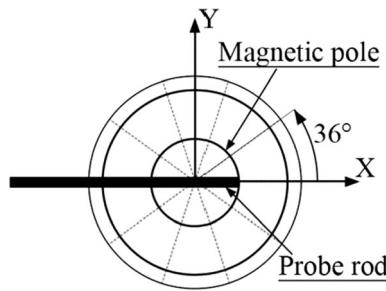


Fig. 2 Measurement method for each 36° rotation

area down to $\phi 30$ mm. The design specifications for the electromagnets discussed in this article were as follows: iron frame parameters: outer diameter 65 mm, inner diameter 57 mm, height 50 mm, thickness 10 mm; magnetic pole parameters: outer diameter 30–55 mm, thickness 5 mm; construction material for iron frame and magnetic pole: SUM24L (12L14); coil parameters: wire diameter 0.2 mm, coil number 2450, resistance $75\ \Omega$, applied direct current power (DC) 24 V, current 0.32 A.

Fig. 3 Measured Gaussian values for magnetic pole surface areas of $\phi 30$ mm and $\phi 55$ mm

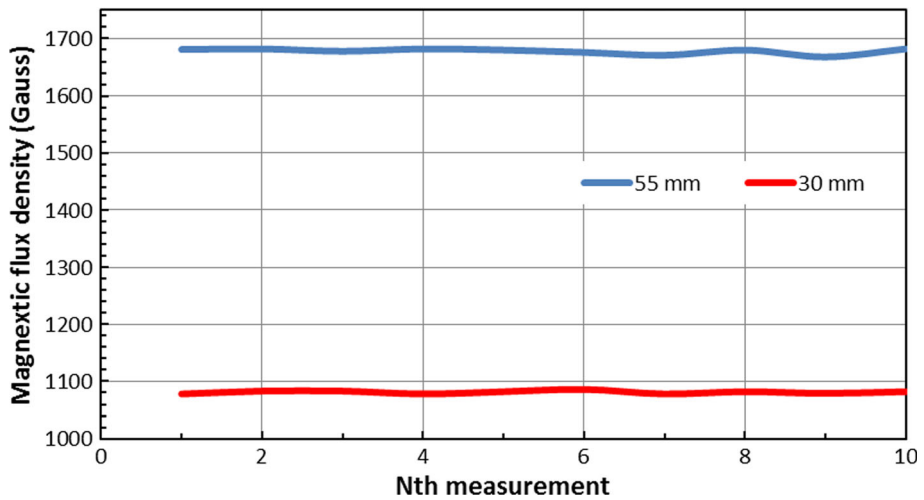
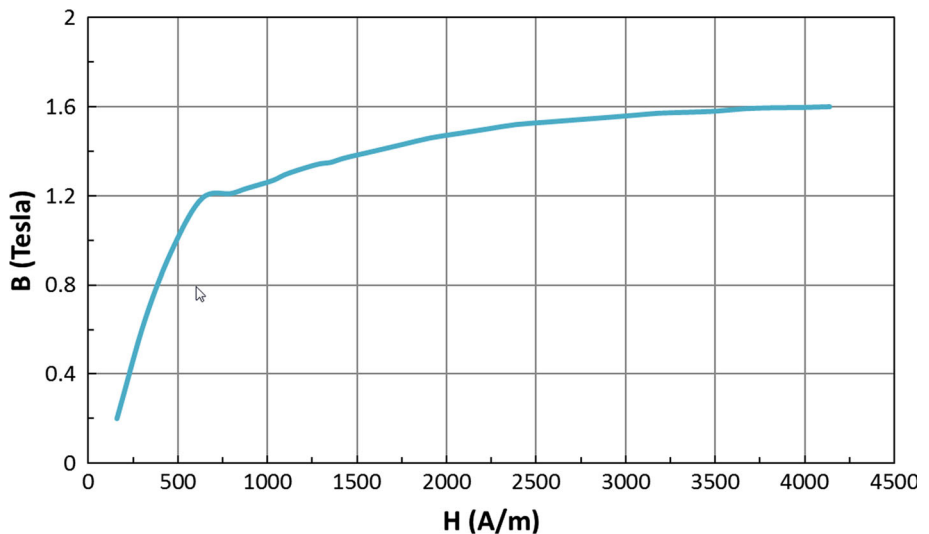


Fig. 4 BH curve of fast-cutting steel (SUM24L)



2.1 Comparison of experimental measurement results and finite element analysis results

For the type of electromagnet holding device shown in Fig. 1, we first utilized a Gauss instrument to measure the surface Gauss (G) value after applying a DC of 24 V to the coils. The measurement method is shown in Fig. 2. There were two types of magnetic pole surface diameters for the research sample prototype: $\phi 55$ mm and $\phi 30$ mm. The electromagnets were measured after each 36° rotation using a fixed probe, as presented in Fig. 3. For the magnetic pole cross-sectional area of $\phi 30$ mm, the average value was 1081 G, while for $\phi 55$ mm, it was 1678 G.

The electromagnetic holding device was constructed using fast-cutting steel for the magnetic pole and iron frame. We used JIS SUM24L (called SAE 12L24 in the US), a low-carbon steel. The BH curve graph for this type of steel is shown in Fig. 4. This study will use the finite element software of ANSYS Maxwell 16.0 to simulate the

surface magnetic lines in order to observe whether the predicted results matched the experimental results. In ANSYS-Maxwell, the Eqs. (1)–(4), named as Ampère equation, Faraday equation, Gauss's law and Gauss's law for magnetism, are used to solve the electromagnetic field problems with appropriate boundary and initial conditions:

$$\nabla \times H = J + \frac{\partial D}{\partial t} \quad (1)$$

$$\nabla \times E = - \frac{\partial B}{\partial t} \quad (2)$$

$$\nabla \cdot E = \rho \quad (3)$$

$$\nabla \cdot B = 0 \quad (4)$$

where H is the magnetic field; J is the total electric current density; D is the electric displacement field; E is the electric field; B is the magnetic field; ρ is the total electric charge density. Therefore, based on these two types of

experimental sample specifications, we used ANSYS Maxwell finite element software to simulate the surface magnetic lines in order to observe whether the predicted results matched the experimental results. The comparisons are shown in Figs. 5 and 6.

The simulated magnetic line distribution for the electromagnetic device with a magnetic pole surface area of $\phi 55$ mm is presented in Fig. 5. Because the magnetic pole board of this type of electromagnetic device is used as the attachment surface, the maximum magnetic flux density value is located in area "A" in Fig. 5a. For ease of interpretation, we present an enlargement of area "A" in Fig. 5b. Analysis results show that the maximum magnetic flux density value is located at "A". By cross-referencing the color of the arrows in Area "A" to the table located in the upper left corner, we know the magnetic flux density is 1650–1800 G. The simulated magnetic line distribution for the electromagnetic device whose cross-sectional surface

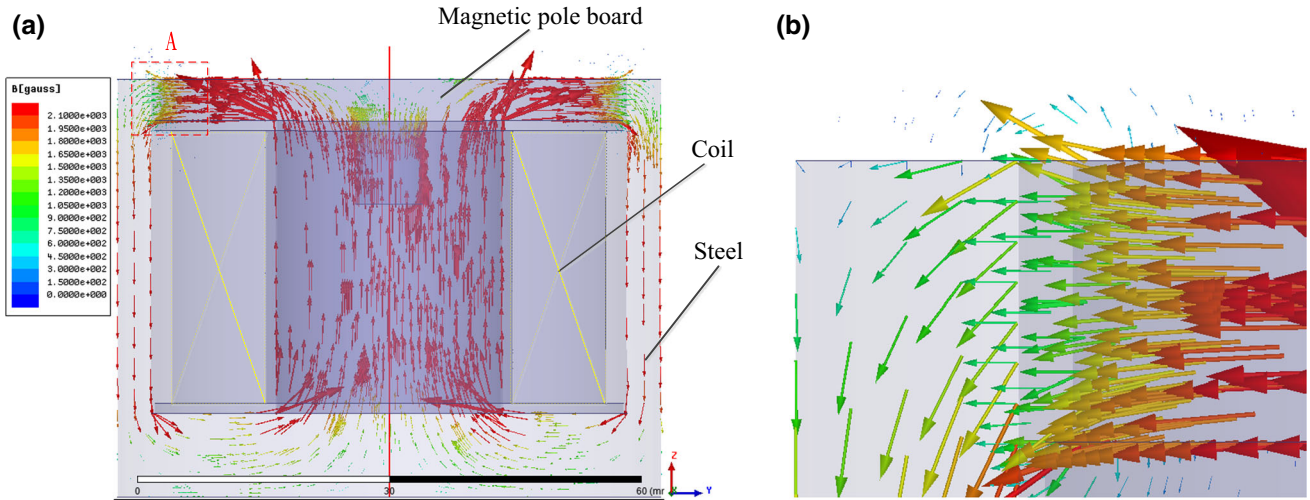


Fig. 5 Magnetic pole surface area $\phi 55$ mm of magnetic chuck: **a** magnetic line simulation graph, **b** enlarged view of area A

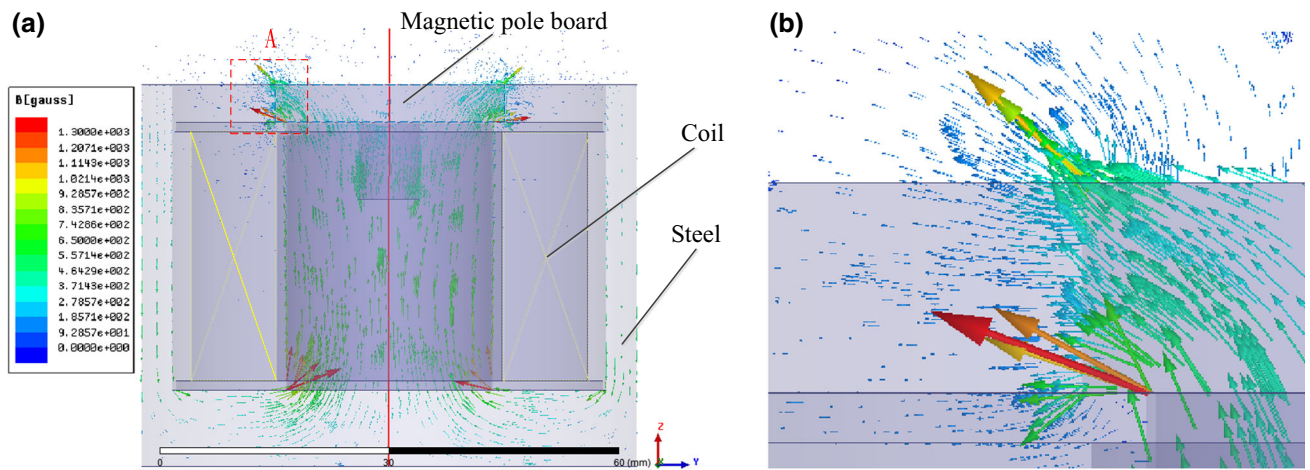


Fig. 6 Magnetic pole surface area $\phi 30$ mm of magnetic chuck: **a** magnetic line simulation graph, **b** enlarged view of area A

area is $\phi 30$ mm is shown in Fig. 6. Similarly, the maximum magnetic flux density occurs in area “A” in Fig. 6a. Enlargement of this area (shown in Fig. 6b) demonstrates that the magnetic flux density is 1021–1143 G.

In addition, we compared the ANSYS Maxwell finite element simulation results by reading the magnetic flux density value of the point located at coordinate (0, y, 50) mm, with various y-axis values; the results are shown in Fig. 7. Comparison of the experimental results with the simulated results shows that for the surface area of $\phi 55$ mm, the average measured magnetic force is 1678 G, while the average maximum magnetic flux density in the simulated results is 1670 G. For a surface area of $\phi 30$ mm, the average measured maximum magnetic flux density is 1081 G, compared with 1039 G in the simulated results. Overall, the simulated results conform to the experimental results. Furthermore, when a 24 Vdc voltage is applied to

electromagnet holding device, the current of the coils is about 0.32 A and its temperature distribution by simulation is shown in Fig. 8. Note that the maximum operated temperature is about 46.4 °C in steady state response. Therefore, in this article we therefore will use the simulation parameters and ANSYS Maxwell finite element software to analyze the design of the electromagnetic holding device.

2.2 Simulation studies for various magnetic pole surface areas

Based on the simulation results shown in Figs. 5 and 6, we further investigated the effect of varying the magnetic pole surface diameter from $\phi 55$ mm to $\phi 30$ mm, in light of the maximum Gauss values of the magnetic pole surface. The maximum and minimum magnetic flux density values and their locations on the surface of the magnetic pole are

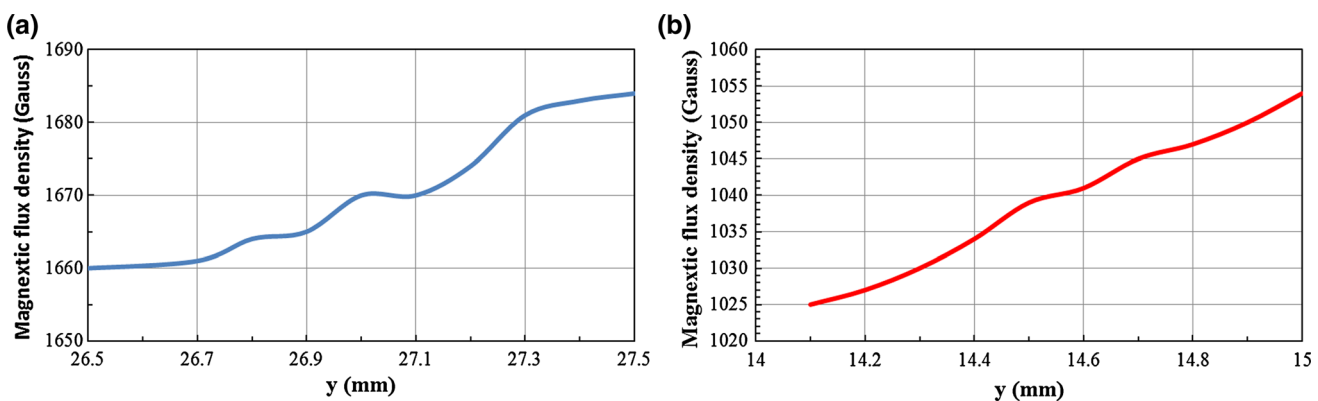


Fig. 7 Maximum magnetic flux density value in the simulation results for magnetic pole surface areas of **a** $\phi 55$ and **b** $\phi 30$ mm

Fig. 8 Temperature distribution of electromagnet holding device when 24 Vdc is applied to the coils

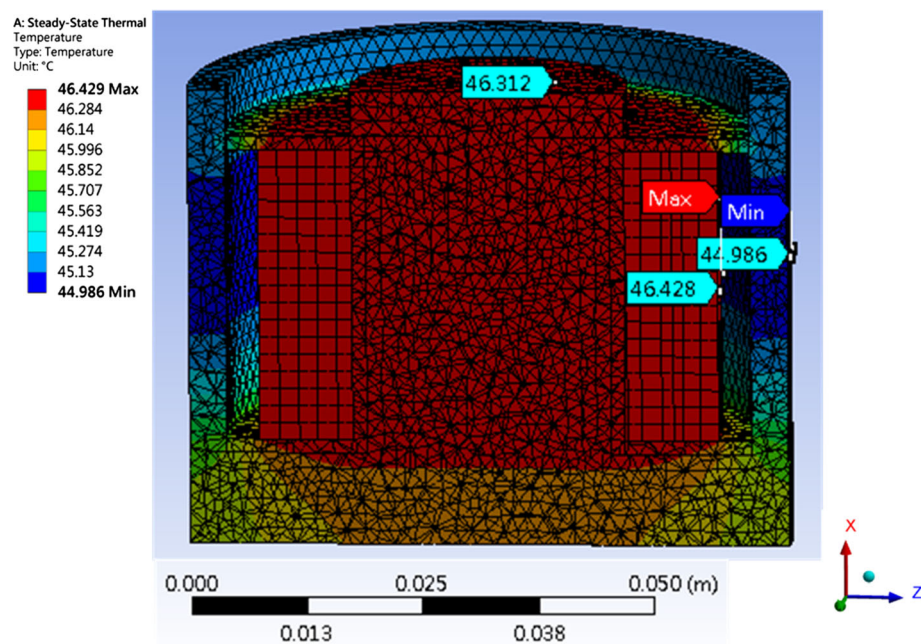
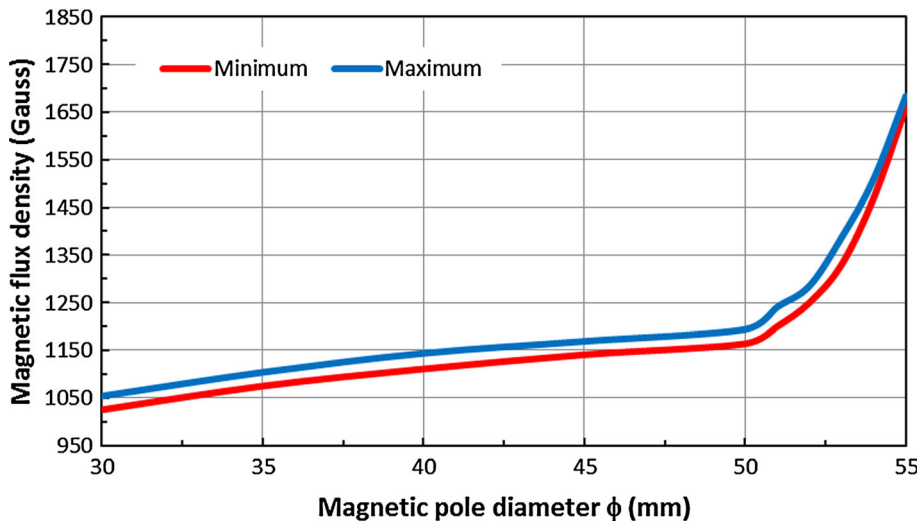


Fig. 9 Simulation graph for magnetic pole surface area and magnetic flux density



shown in Fig. 9. It is clear from the analysis results that the $\phi 55$ mm magnetic pole surface has the largest maximum and minimum values. As the diameter gradually decreases from $\phi 55$ mm, the Gauss value on the magnetic pole also gradually decreases. Notably, the largest drop in magnetic force occurs from $\phi 55$ mm to $\phi 50$ mm. This is because the location with the highest magnetic flux density is simultaneously affected by the magnetic pole and the magnetic yoke. However, as the magnetic pole surface area drops below $\phi 50$ mm, the distance between the magnetic pole and the iron frame gradually creates an air gap, reducing the influence of the magnetic pole and the yoke. Simultaneously, the magnetization effect of the magnetic flux density and magnetic pole on the iron frame is weakened. The Gauss value at location “A” will only be affected by a single magnetic pole, so the reduction in surface area with respect to the Gauss value of the magnetic flux density exhibits a stable linear relationship.

2.3 Simulation studies for magnetic permeability distance

In addition to magnetic flux density (Gauss), another factor that affects the strength of the magnetic force for attracting an object is the magnetic permeability distance: the maximum distance at which an object is affected by a magnet. In Fig. 10, “H” indicates the magnetic permeability distance. Based on magnetization principles, the larger the “H”, the stronger the effect exerted by the magnetic pole on the magnetic substance, so the more the magnetic dipoles are affected. This is why sometimes a magnet with a low Gauss value can attract a heavier object. Figures 11 and 12 present the simulated magnetic divergence results for magnetic pole areas of $\phi 30$ and $\phi 55$ mm. Figure 11 shows the magnetic line divergence region for the $\phi 30$ mm area. Note that its overall appearance is a semicircular arc.

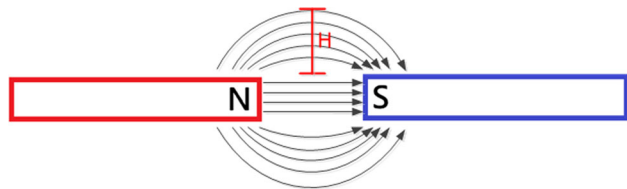


Fig. 10 Schematic diagram of magnetic divergence distance

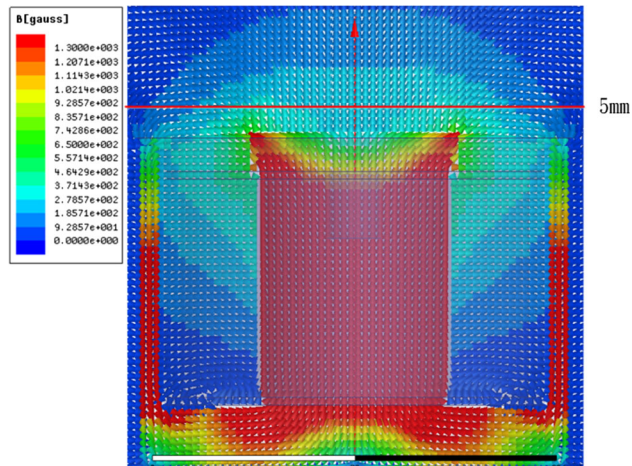


Fig. 11 Magnetic divergence simulation diagram for magnetic pole surface area $\phi 30$ mm (24 V)

The red horizontal line marks where the distance from the surface of the magnetic pole is 5 mm; the magnetic flux density can be looked up in the table on the left in Fig. 11. The magnetic flux density is approximately 400–600 G. Similarly, Fig. 12 indicates the magnetic permeability distance for the surface area of $\phi 55$ mm. A gap is observable in the center. The red horizontal line in Fig. 12 also marks a distance of 5 mm from the surface of the magnetic pole; here, the magnetic flux density is clearly much lower than with the $\phi 30$ mm area. Based on the color

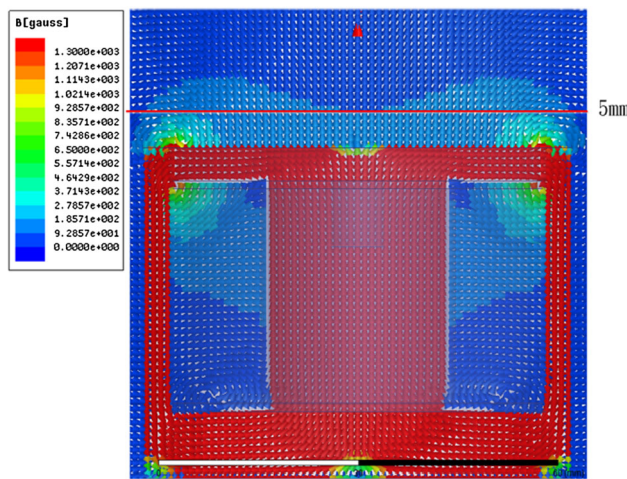


Fig. 12 Magnetic divergence simulation diagram for magnetic pole surface area $\phi 55$ mm (24 V)

indicators, the corresponding magnetic flux density is 278–371 G. Therefore, when the magnetic pole surface area is $\phi 55$ mm, the magnetic divergence at the center of the magnetic pole is not very strong, so when attracting objects, some of the magnetic areas are not available. This is why at 24 V, the $\phi 55$ mm magnetic pole attracted less weight than the $\phi 30$ mm pole.

3 Effect of varying iron frame thickness on the electromagnet

The iron frame thickness in the previous section was fixed at 4 mm. Now we investigate how varying the iron frame thickness affects the magnetic line distribution of the electromagnetic holding device for surface areas of ϕ

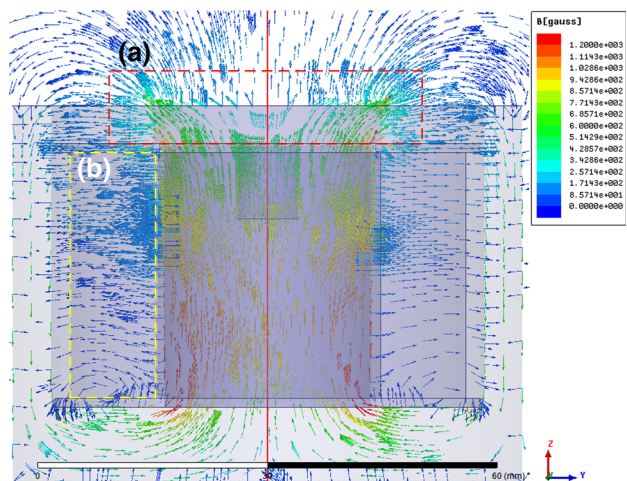


Fig. 13 Magnetic simulation diagram of electromagnetic holding device with magnetic pole surface area $\phi 30$ mm and iron frame thickness 5 mm

30 mm, $\phi 45$ mm, and $\phi 55$ mm. The simulation results for a $\phi 30$ mm surface area and a 5 mm iron frame thickness are shown in Fig. 13. The magnetic lines are sparser in the area marked "a" because more magnetic lines are being guided toward the edge of the iron frame, which can be observed in the area marked "b". Figure 14 illustrates the maximum and minimum lines when the thickness of the iron frame is varied for a surface area of $\phi 30$ mm; the largest magnetic strength occurs when the iron frame thickness is 4.5 mm, making it the optimal thickness for this surface area.

Similarly, Fig. 15 shows the variations in magnetic flux density with different iron frame thicknesses for a $\phi 45$ mm surface area. The optimal density is achieved with 4 mm thickness. When the surface area is $\phi 30$ mm, the larger air gap leads to greater magnetic resistance in the magnetic circuit, so reduction in the iron frame has less effect on the overall magnetic resistance. On the other hand, increasing the iron frame thickness has a greater effect on the magnetic flux density because it affects the magnetic line guidance. The result is that the magnetic flux density for the electromagnet with a 5 mm iron frame thickness is less than with a 3 mm thickness. As the magnetic pole surface area increases to $\phi 45$ mm, the air gap in the magnetic circuit decreases, as does the magnetic resistance. In this case, decreasing the thickness will increase the magnetic resistance in the magnetic circuit, so the performance with a 3 mm thickness will be lower than with a 5 mm thickness.

Figure 16 shows the effect of varying the iron frame thickness with a surface area of $\phi 55$ mm. In this case, the magnetic pole surface is very close to the inner diameter of the iron frame ($\phi 57$ mm), so the effect of having small magnetic resistance and large magnetic permeability is quite pronounced. The magnetic flux density reaches a maximum value of 1730 G when the iron frame thickness is 4.5 mm. Even though the Gauss value at the surface is far higher than in the former two scenarios, it is clear from the magnetic permeability simulations that the magnetic permeability of the electromagnetic holding device shown in Fig. 17 is inferior, and most of the magnetic lines are enclosed in the magnetic circuit. As a result, when a magnetic object is held, fewer magnetic lines participate in forming the magnetic circuit, so the electromagnet has less holding force.

In the three simulation models discussed previously, as the iron frame thickness increases, the magnetic lines at the center of the electromagnetic holding device become diffuse. On the other hand, when the iron frame is too thin, the resistance in the circuit increases, thereby lowering the circuit's permeability. Under these conditions, the key when adjusting the frame thickness is to avoid causing the magnetic lines to become diffuse too early, while at the

Fig. 14 Relational graph of magnetic frame thickness and magnetic strength for electromagnetic holding device with magnetic pole surface area $\phi 30$ mm

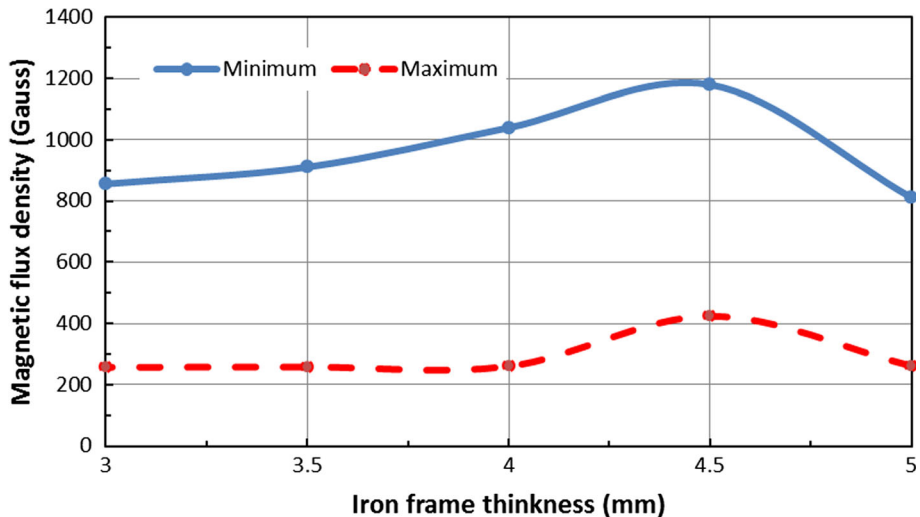


Fig. 15 Relational graph of magnetic frame thickness and magnetic strength for electromagnetic holding device with magnetic pole surface area $\phi 45$ mm

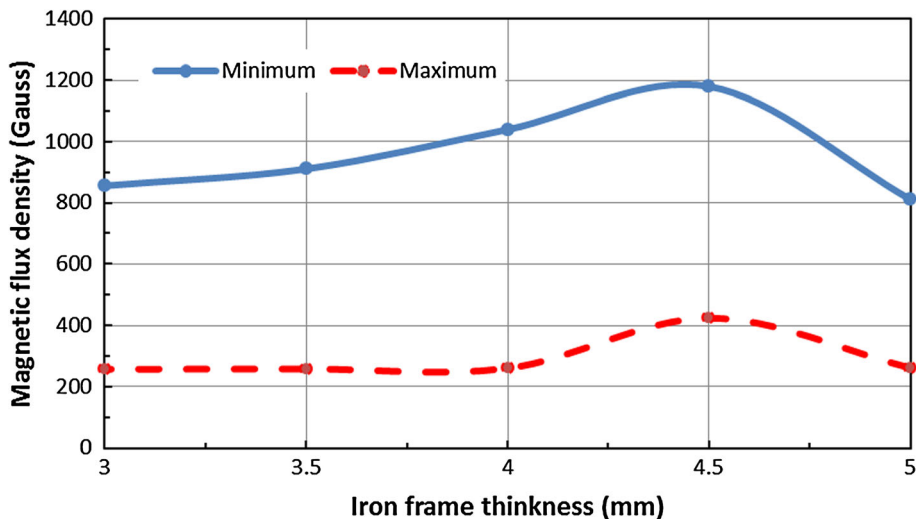
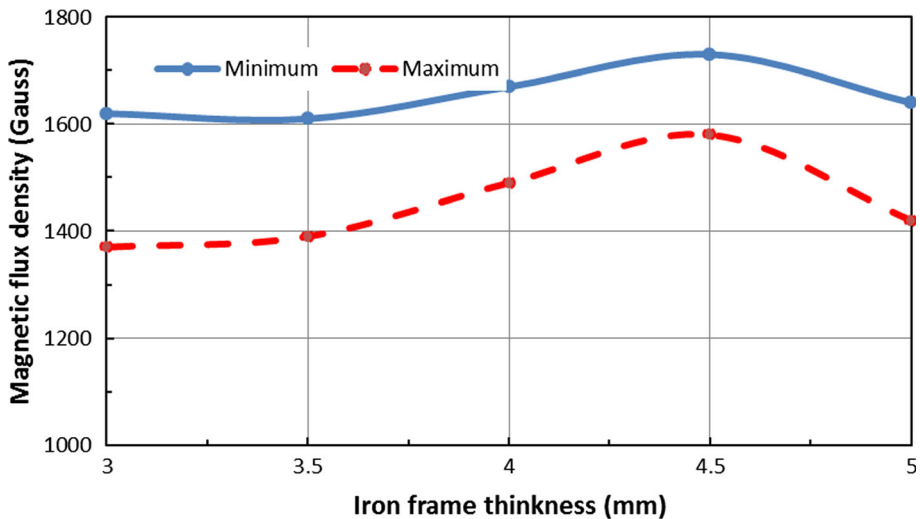


Fig. 16 Relational graph of magnetic frame thickness and magnetic strength for electromagnetic holding device with magnetic pole surface area $\phi 55$ mm



same time not increasing the overall resistance in the circuit. This is why the magnetic resistance is the foremost

design consideration when the electromagnetic pole surface is $\phi 55$ mm. On the other hand, when the

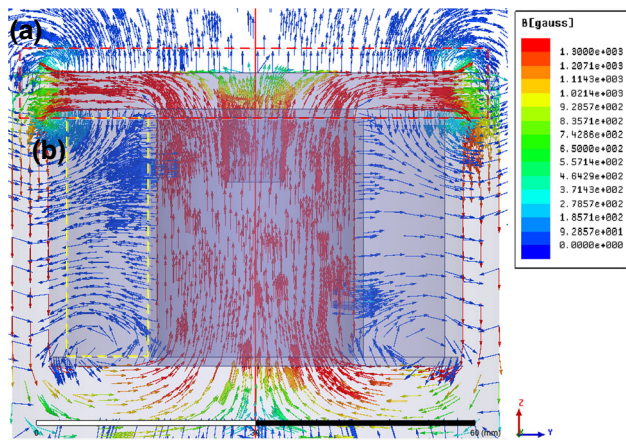


Fig. 17 Magnetic simulation diagram for electromagnetic holding device with magnetic pole surface area $\phi 55$ mm and iron frame thickness 5 mm

electromagnetic surface is $\phi 30$ mm, the design priority is to avoid having the magnetic lines become diffuse too quickly.

4 Experimental results

4.1 Attraction strength of electromagnetic holding devices

We investigated the holding strengths of electromagnetic holding devices with magnetic pole surface areas of $\phi 55$ mm and $\phi 30$ mm. The polished surface of the electromagnetic pole is shown in Fig. 18. The surface should be smooth to ensure that the iron frame and the magnetic pole surface are on the same horizontal plane. If they are not, the contact plane between the object and the electromagnet will be a point or a line instead of a surface, drastically decreasing the performance of the electromagnetic holding device.

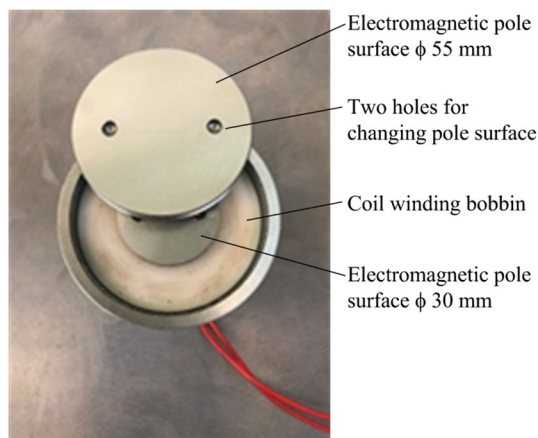


Fig. 18 Ground surface and pole plate

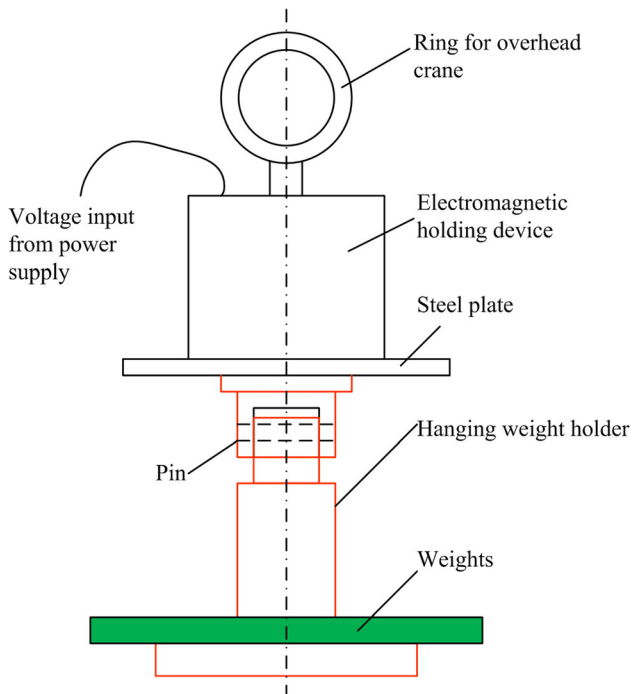


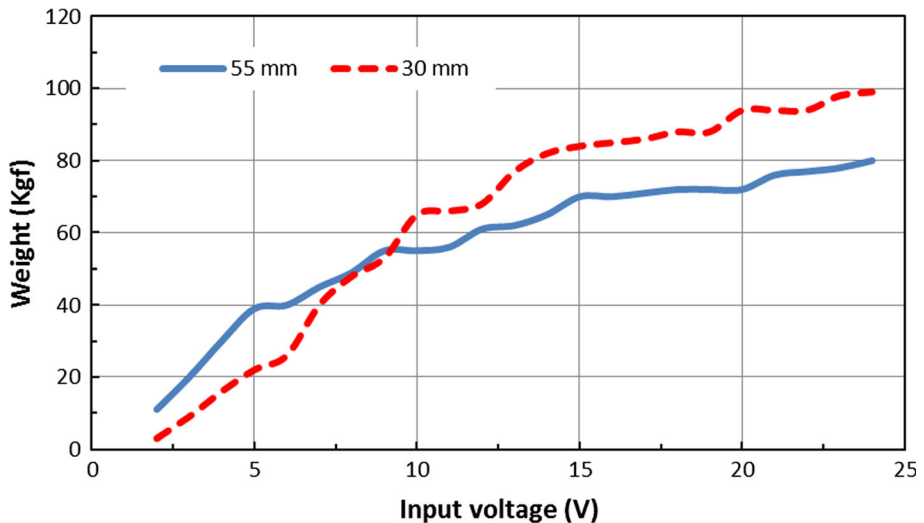
Fig. 19 Experimental testing system

The overall testing system is illustrated in Fig. 19. The fixture weight used for testing is about 1108.4 g. Similar to the electromagnetic pole surface, the end of the fixture holding the object must be level and smooth. The holding surface dimensions must exceed the outer diameter of the electromagnet holding device to ensure the generated magnetic force completely covers the holding surface. The test method was to gradually add weights. Note that a power supply was used to provide an adjustable voltage input for the electromagnetic device in 1 V increments. The power output of the electromagnet was modulated by the adjustable power supply. A crane arm was used to position the object during testing.

The experimental results for the weight-holding experiments involving electromagnets with magnetic pole surface areas of $\phi 55$ mm and $\phi 30$ mm are presented in Fig. 20. With the $\phi 55$ mm surface area and under low-voltage conditions (1–9 V), the electromagnet held more weight than with the $\phi 30$ mm surface area; for example, at 2 V, the $\phi 55$ mm electromagnet held four times more weight. The difference decreased as the input voltage increased, and by 9 V, the comparative strengths had reversed. When the input voltage reached 24 V, the $\phi 30$ mm electromagnet could hold 19 kg more than the $\phi 55$ mm one.

When we consider factors that influence magnetic strength, what comes to mind first are changes in Gauss value. These changes under different input voltages for the $\phi 30$ and $\phi 55$ mm electromagnets are shown in Fig. 21; the

Fig. 20 Measured adsorbed holding weight of electromagnetic holding devices with magnetic pole surface areas $\phi 55$ mm and $\phi 30$ mm



data clearly show a linear increasing relationship between Gauss values measured at the electromagnetic pole surfaces and input voltages. Because $\phi 55$ mm is larger than $\phi 30$ mm, the former electromagnet's measured Gauss value is always greater than the latter's. The difference reaches 600 G when the input voltage is 24 V, but the maximum holding weight of the $\phi 55$ mm electromagnet is less—as noted above, the $\phi 30$ mm electromagnet can hold 19 kg more weight. It is therefore clear that the main factor influencing the holding weight of the electromagnetic holding device is not the magnitude of the surface Gauss value but instead the magnetic permeability distance of the electromagnetic holding device.

4.2 Measurement of magnetic permeability

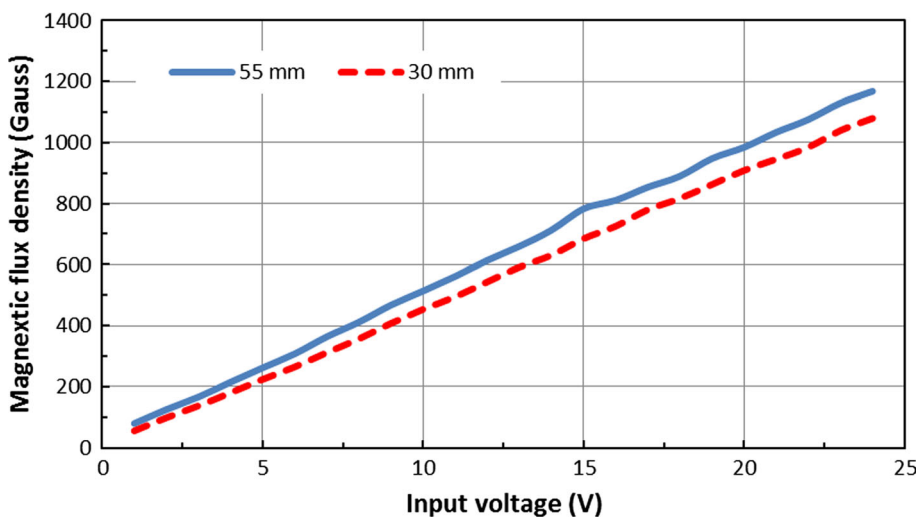
The method used for measuring the magnetic permeability of the electromagnetic holding devices is illustrated in Fig. 22. We used a Gauss meter to measure the Gauss

value at points located at certain heights above the magnetic pole surface and a height gauge to measure the distance between the points and the magnetic pole surface. Note that we placed the probe of the Gauss meter in front of a copper bar, replacing the magnetic metal with copper, which would not interact and form a magnetic circuit, preventing mutual interference between the magnetic objects. This allowed us to obtain more accurate data, ensure we could stabilize the increase rate, and prevent the probe from shifting horizontally.

The measured Gauss values for distances 5 and 10 mm from the magnetic pole surface are provided in Fig. 23. At low voltages, there was not much difference between the Gauss values for electromagnets with different magnetic pole surface areas, but the differences increased dramatically once the input voltage reached 9 V and continued thereafter, hitting a maximum value at 24 V.

In addition, it is worth noting that with the $\phi 30$ mm electromagnet, as the input voltage increased, so did the

Fig. 21 Measured Gauss values with respect to input voltage for electromagnetic holding devices with magnetic pole surface areas $\phi 55$ mm and $\phi 30$ mm



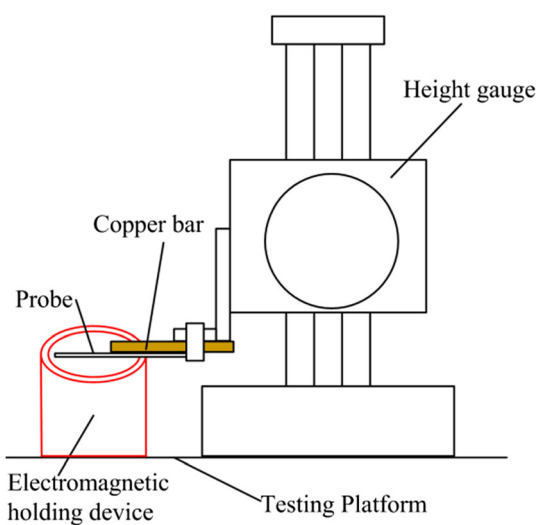
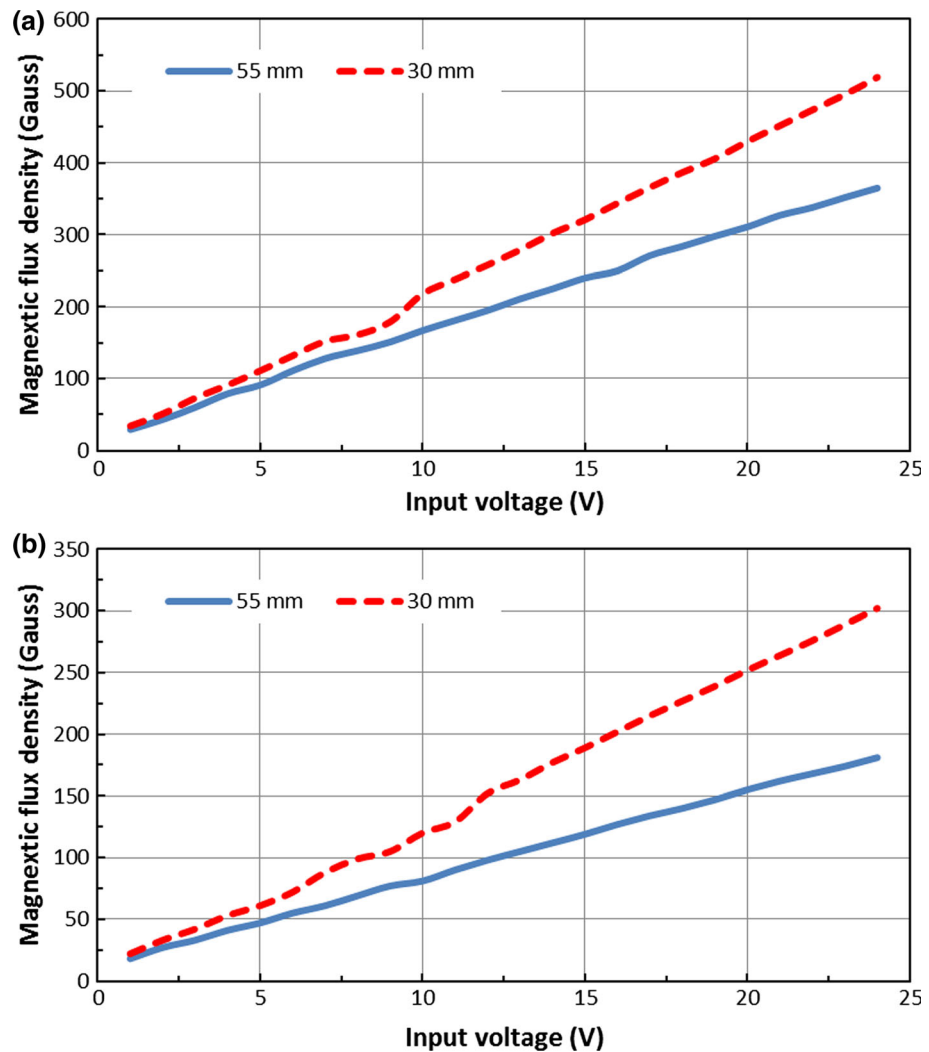


Fig. 22 Height measurement component set up for Gauss meter

Fig. 23 Magnetic distance measurement of electromagnetic holding devices with magnetic pole surface areas $\phi 55$ mm and $\phi 30$ mm: **a** 5 mm and **b** 10 mm from the pole surface



magnetic permeability. However, for the $\phi 55$ mm electromagnet, the magnetic permeability did not increase with greater input voltage. Therefore, based on the design specifications of the electromagnetic holding devices studied in this article, an input voltage of 9 V was the balance point between magnetic strength and magnetic permeability. Once the balance point was passed, the effect of magnetic permeability on the holding weight continued to increase, as explained in Sect. 2, showing that magnetic force tended to choose the shorter route. The increase in voltage in the N magnetic pole did not permeate outward but instead chose to pass through the iron frame and flow towards the S magnetic pole to form a magnetic circuit. This is why the holding weight for the electromagnetic holding device with a large magnetic pole surface area did not increase with the rising input voltage.

5 Conclusions

In this paper, we have successfully used ANSYS Maxwell finite element software to assist in analyzing the design specifications of commonly used electromagnetic holding devices. With regard to the electromagnetic holding devices studied in this article, the holding strength generated from the magnetic permeability was balanced at 9 V. For a magnetic pole surface area of $\phi 55$ mm, the holding strength was greater when the input voltage was below 9 V. Above 9 V, a magnetic pole surface area of $\phi 30$ mm yielded greater holding strength due to the effect of magnetic permeability. Experimental results also demonstrated that when the object to be held is less than 50 kg and one wishes to avoid the problem of heat generation due to high voltage, increasing the magnetic pole surface area is a solution. Furthermore, the Gauss value can be increased without changing the electromagnet's external dimensions by increasing the magnetic pole surface area, but this may sacrifice the divergent flux area of the electromagnetic holding device. When changing the iron frame's thickness, one must consider the overall balance of the magnetic circuit. Decreasing the frame thickness will increase the circuit's magnetic resistance and lower the magnetic permeability, whereas increasing it will lead to diffusion of the surface magnetic lines. From the experiment results, the optimal iron frame thickness is recommended as 12–13% of the electromagnet's outer diameter, to reach the effect of the maximum magnetic flux density. In the future, we will extend the research results in this article to electromagnetic holding devices with permanent magnets or electromagnetic brakes.

References

Alizadeh HV, Boulet B (2016) Analytical calculation of the magnetic vector potential of an axisymmetric solenoid in the presence of iron parts. *IEEE Trans Magn* 52:8201104

- Duchaud J-L, Hlioui S, Louf F, Ojeda J, Gabsi M (2015) Modeling and optimization of a linear actuator for a two-stage valve tappet in an automotive engine. *IEEE Trans Veh Technol* 64:4441–4448
- Han DK, Chang JH (2016) Design of electromagnetic linear actuator using the equivalent magnetic circuit method. *IEEE Trans Magn*. <https://doi.org/10.1109/tmag.2015.2498198>
- Kim J, Chang J (2007) A new electromagnetic linear actuator for quick latching. *IEEE Trans Magn* 43:1849–1852
- Li C, Yang H, Jenkins LL, Dean RN, Flowers GT, Hung JY (2016) Enhanced-performance control of an electromagnetic solenoid system using a digital controller. *IEEE Trans Control Syst Technol* 24:1805–1811
- Liu Q, Bo H, Qin B (2010) Experimental study and numerical analysis on electromagnetic force of direct action solenoid valve. *Nucl Eng Des* 240:4031–4036
- Liu C-T, Chiu Y-W, Hwang C-C (2016) Designs and feasibility assessments of an integrated linear electromagnetic actuator for cold roll mill applications. *IEEE Trans Ind Appl* 52:2693–2699
- Mansfield AN (2006) Electromagnets: their design and construction. Watchmaker Publishing, Washington. ISBN 9781933998053
- Mercorelli P, Lehmann K, Liu S, Muamer H, Reimann B (2003) Control of an electromagnetic linear actuator using flatness property and systems Inversion. In: 2003 European control conference (ECC), Cambridge, UK, 1–4 Sept., 2003
- Sun Z-Y, Li G-X, Wang L, Wang W-H, Gao Q-X, Wang J (2016) Effects of structure parameters on the static electromagnetic characteristics of solenoid valve for an electronic unit pump. *Energy Convers Manag* 113:119–130
- Wang L, Li G-X, Xu C-L, Xi X, Wu X-J, Sun S-P (2016) Effect of characteristic parameters on the magnetic properties of solenoid valve for high-pressure common rail diesel engine. *Energy Convers Manag* 127:656–666
- Wu CH, Grant CV, Cook GA, Park SH, Opella SJ (2009) A strip-shield improves the efficiency of a solenoid coil in probes for high-field solid-state NMR of lossy biological samples. *J Magn Reson* 200:74–80. <https://doi.org/10.1016/j.jmr.2009.06.004>
- Zheng J, Song Y, Liu X, Li L, Wan Y, Wan B, Ye M, Wu H (2015) Concept design of the CFETR central solenoid. *Fusion Eng Des* 91:30–38
- Zhu J, Chang S (2012) Modeling and simulation for application of electromagnetic linear actuator direct drive electro-hydraulic servo system. In: 2012 IEEE international conference on power and energy (PECon), Kota Kinabalu Sabah, Malaysia, 2–5 December 2012

Publisher's Note Springer Nature remains neutral with regard to jurisdictional claims in published maps and institutional affiliations.

Terms and Conditions

Springer Nature journal content, brought to you courtesy of Springer Nature Customer Service Center GmbH (“Springer Nature”). Springer Nature supports a reasonable amount of sharing of research papers by authors, subscribers and authorised users (“Users”), for small-scale personal, non-commercial use provided that all copyright, trade and service marks and other proprietary notices are maintained. By accessing, sharing, receiving or otherwise using the Springer Nature journal content you agree to these terms of use (“Terms”). For these purposes, Springer Nature considers academic use (by researchers and students) to be non-commercial.

These Terms are supplementary and will apply in addition to any applicable website terms and conditions, a relevant site licence or a personal subscription. These Terms will prevail over any conflict or ambiguity with regards to the relevant terms, a site licence or a personal subscription (to the extent of the conflict or ambiguity only). For Creative Commons-licensed articles, the terms of the Creative Commons license used will apply.

We collect and use personal data to provide access to the Springer Nature journal content. We may also use these personal data internally within ResearchGate and Springer Nature and as agreed share it, in an anonymised way, for purposes of tracking, analysis and reporting. We will not otherwise disclose your personal data outside the ResearchGate or the Springer Nature group of companies unless we have your permission as detailed in the Privacy Policy.

While Users may use the Springer Nature journal content for small scale, personal non-commercial use, it is important to note that Users may not:

1. use such content for the purpose of providing other users with access on a regular or large scale basis or as a means to circumvent access control;
2. use such content where to do so would be considered a criminal or statutory offence in any jurisdiction, or gives rise to civil liability, or is otherwise unlawful;
3. falsely or misleadingly imply or suggest endorsement, approval , sponsorship, or association unless explicitly agreed to by Springer Nature in writing;
4. use bots or other automated methods to access the content or redirect messages
5. override any security feature or exclusionary protocol; or
6. share the content in order to create substitute for Springer Nature products or services or a systematic database of Springer Nature journal content.

In line with the restriction against commercial use, Springer Nature does not permit the creation of a product or service that creates revenue, royalties, rent or income from our content or its inclusion as part of a paid for service or for other commercial gain. Springer Nature journal content cannot be used for inter-library loans and librarians may not upload Springer Nature journal content on a large scale into their, or any other, institutional repository.

These terms of use are reviewed regularly and may be amended at any time. Springer Nature is not obligated to publish any information or content on this website and may remove it or features or functionality at our sole discretion, at any time with or without notice. Springer Nature may revoke this licence to you at any time and remove access to any copies of the Springer Nature journal content which have been saved.

To the fullest extent permitted by law, Springer Nature makes no warranties, representations or guarantees to Users, either express or implied with respect to the Springer nature journal content and all parties disclaim and waive any implied warranties or warranties imposed by law, including merchantability or fitness for any particular purpose.

Please note that these rights do not automatically extend to content, data or other material published by Springer Nature that may be licensed from third parties.

If you would like to use or distribute our Springer Nature journal content to a wider audience or on a regular basis or in any other manner not expressly permitted by these Terms, please contact Springer Nature at

onlineservice@springernature.com